Earth and Planetary Science Letters 495 (2018) 79–86

Contents lists available at ScienceDirect

Earth and Planetary Science Letters

www.elsevier.com/locate/epsl

Lithospheric layering beneath the contiguous United States constrained by S-to-P receiver functions

Lin Liu, Stephen S. Gao *

Geology and Geophysics Program, Missouri University of Science and Technology, Rolla, MO 65409, USA

ARTICLE INFO

Article history:
Received 12 February 2018
Received in revised form 30 April 2018
Accepted 3 May 2018
Available online 16 May 2018
Editor: M. Ishii

Keywords:
lithosphere
continental crust
lithospheric thickness
receiver function

ABSTRACT

To image upper mantle seismic discontinuities beneath the contiguous United States, a total of 284,121 S-to-P receiver functions (SRFs) recorded by 3,594 broadband seismic stations in the EarthScope Transportable Array and other permanent and temporary deployments are stacked in circular bins of 2° in radius. A robust negative arrival, representing a sharp discontinuity of wave speed reduction with depth, is visible in virtually all the stacked traces in the depth range of 30–110 km. Beneath the western U.S., the mean depth of this discontinuity is 69±17 km, and beneath the eastern U.S., it is 76±5 km, both are comparable to the depth of the tomographically-determined lithosphere–asthenosphere boundary (LAB). In contrast, the depth of the discontinuity beneath the stable cratonic region of the central U.S. is 87 ± 6 km, which is significantly shallower than the ∼250 km LAB depth determined by seismic tomography. Based on the amplitude of the corresponding arrival in the SRFs and findings from previous seismic tomography and mantle xenolith studies, this discontinuity beneath the central U.S. is interpreted as the top of an intra-lithospheric low wave speed, probably phlogopite-rich layer. The observations provide new constraints on a number of regional scale tectonic processes, such as lithospheric stretching in the Texas–Louisiana Gulf Coastal Plain and the Basin and Range Province, and possible lithospheric basal erosion beneath the northeastern U.S.

1. Introduction

Reliably mapping the thickness and layering of the lithosphere, which is the outermost rigid shell of the Earth, is essential in understanding upper mantle structure and dynamics (McKenzie and Priestley, 2008). Two of the most frequently employed seismological techniques for investigating lithospheric thickness and layering are surface wave tomography (McKenzie and Priestley, 2008; Bedle and van der Lee, 2009; Schaeffer and Lebedev, 2014; Caló et al., 2016) and stacking of receiver functions which are P-to-S or S-to-P converted phases (P_s and S_p, respectively) from wave speed discontinuities at the bottom of or inside the lithosphere (Rychert and Shearer, 2009; Fischer et al., 2010; Kind et al., 2012). Surface wave tomography can detect gradual variations in wave speed gradient, but is insensitive to sharp discontinuities due to low vertical resolution (Li et al., 2007; Rychert et al., 2007). In contrast, P-to-S receiver functions are widely used for imaging the Moho and mantle transition zone discontinuities (Zhu and Kanamori, 2000; Gao and Liu, 2014; Liu et al., 2017), but are not effective to study lithospheric discontinuities because of the strong Moho multiples in the expected time window of the arrivals associated with the discontinuities (Faber and Müller, 1980). Instead, lithospheric discontinuities are commonly imaged using S-to-P receiver functions (SRFs), in which the S_p arrivals are precursors to the direct S-wave. Because the Moho multiples appear after the direct S-wave, a separation of the primary converted phases and the multiples is expected on the SRFs (Faber and Müller, 1980). Relative to surface wave tomography, SRF stacking has the disadvantage that only sharp discontinuities can be detected. Tests suggest that a discontinuity that is 50 km or thicker cannot generate observable S-to-P converted phases (Kumar et al., 2012).

Beneath the contiguous United States (Fig. 1), the observed lithospheric thickness from most surface wave tomography studies demonstrates similar spatial variations, with values as small as less than 70 km beneath the western U.S., 90–150 km along the Rocky Mountains, Colorado Plateau, and Appalachians, and about 250 km beneath the tectonically stable cratonic region of the central U.S. (McKenzie and Priestley, 2008; Bedle and van der Lee, 2009; Schaeffer and Lebedev, 2014). The observed spatial variations of lithospheric thickness correspond well with measurements from shear wave speed gradient (Yuan and Romanowicz, 2010), electrical conductivity (Murphy and Egbert, 2017), mantle xenolith

* Corresponding author.
E-mail address: sgao@mst.edu (S.S. Gao).

https://doi.org/10.1016/j.epsl.2018.05.012
0012-821X/

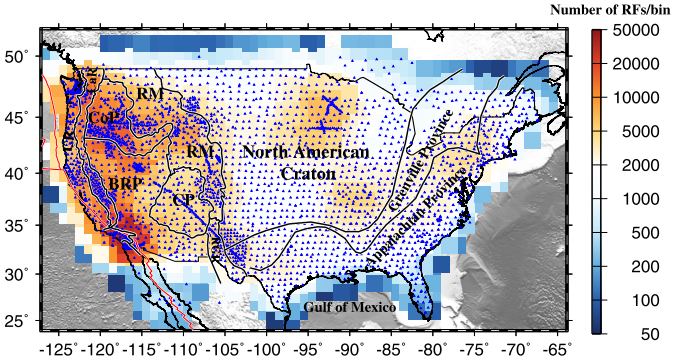

Fig. 1. Number of S receiver functions in radius = 2° circular bins and broadband seismic stations (blue triangles) used in the study. The thick black lines delineate major tectonic provinces. CR: Coast Ranges, CaR: Cascade Range-Sierra Nevada, CoP: Columbia Plateau, BRP: Basin and Range Province, RM: Rocky Mountains, CP: Colorado Plateau, and RGR: Rio Grande Rift (Hoffman, 1988). (For interpretation of the colors in the figure(s), the reader is referred to the web version of this article.)

(Mareschal and Jaupart, 2004), and shear wave splitting (Yang et al., 2014).

A number of SRF studies have been conducted over the past decade to image lithospheric discontinuities beneath North America (Li et al., 2007; Rychert et al., 2007; Abt et al., 2010; Lekić et al., 2011; Kind et al., 2012; Kumar et al., 2012; Levander and Miller, 2012; Lekić and Fischer, 2014; Hansen et al., 2015; Hopper and Fischer, 2015; Reeves et al., 2015). Most previous work report a sharp negative-wave speed discontinuity (NVD) in the depth range of 40–180 km beneath the contiguous U.S. The NVD beneath the western and eastern U.S. has a depth ranging from 40 to 110 km, which is similar to the depth of the lithosphere–asthenosphere boundary (LAB) revealed by surface wave tomography, and is consequently considered as the bottom of the lithosphere (Rychert et al., 2007; Abt et al., 2010; Hansen et al., 2015). In contrast, the depth of the NVD beneath the central U.S. ranges from 80 to 180 km (Kumar et al., 2012; Hansen et al., 2015), which is significantly smaller than the ∼250 km depth determined using surface wave tomography (McKenzie and Priestley, 2008; Bedle and van der Lee, 2009). The NVD is therefore regarded as a mid-lithospheric discontinuity (MLD) rather than the LAB beneath most areas of the central U.S.

The current study is motivated by a number of factors. First, previous SRF studies used none or only part of the EarthScope Transportable Array (TA) stations (Fig. 1), leading to limited station coverage especially for the eastern U.S. Second, there are apparent discrepancies among existing SRF investigations in the resulting depth of the NVD (see Fig. 8 in Hansen et al., 2015 for a comparison of results from four SRF studies). For instance, in the stable cratonic region of the central U.S., the depth is ∼100 km in Kumar et al. (2012) and Hopper and Fischer (2015), but is as large as 160 km in Hansen et al. (2015). Such discrepancies are most likely caused by the different methodologies used by the different studies, as well as the weak signal from the target discontinuities and the consequent uncertainties in reliably identifying the correct arrivals, especially when a small bin size for stacking is used to reach a high lateral resolution (e.g., the radius is about 0.4° in Hansen et al., 2015). In this study, we use a relatively large bin size (radius = 2°) to obtain more reliable results with a comparatively lower resolution for the whole contiguous U.S. Third, while it is known that the stacking amplitude of the negative arrival from the NVD is a significant parameter to quantify the sharpness of the interface to provide additional constraints on the nature of the discontinuities (Abt et al., 2010), spatial variation of the amplitude over the entire study area remains absent. Finally, some of the SRF studies (Li et al., 2007; Kumar et al., 2012; Hansen et al., 2015) briefly discussed the possibility that the negative arrival beneath the Moho could be a side-lobe of the strong S-to-P conversion from the Moho. Although this possibility has been considered as unlikely based on the strong amplitude of the negative arrival and the occasionally independent structure of the Moho and the NVD, a systematic synthetic study to confirm this is still lacking.

In this study we use all the available broadband seismic data recorded prior to January, 2016, including those from all the TA stations, to image the depth of and SRF stacking amplitude associated with lithospheric discontinuities beneath the contiguous U.S., with an unprecedented station coverage for the area. Additionally, we perform synthetic test on the possibility that the observed negative arrival corresponding to the NVD is an artifact from the Moho.

2. Data and methods

The broadband seismograms used in the study are obtained from the Incorporated Research Institutions for Seismology (IRIS) Data Management Center (DMC) using BREQ_FAST. A total of 3,594 stations contributed to the dataset, including 1,667 TA stations which sample the study area with an ∼70 km interval. The seismograms are recorded within a duration of up to 28 yrs, from January 1988 to January 2016, during which all the USArray TA stations have finished their recording in the study area (125°W–65°W and 25°N–50°N). We use the following empirical formula for the cutoff magnitude (M_c) similar to that used by Liu and Gao (2010) to balance the quantity and quality of the requested seismograms, i.e., $M_c = 5.2 + (\Delta - 30.0)/(180.0 - 30.0) - D/700.0$, where Δ is the epicentral distance in degree which is between 60° and 85° for the study, and D is the focal depth in km. The requested seismograms are then trend-removed and band-pass filtered in the frequency band of 0.06–0.6 Hz. Those with a direct S-wave signal-to-noise ratio of 1.5 or greater on the radial component are selected to compute SRFs. The three-component ZNE (vertical, N-S, E-W) seismograms are rotated to LQT (P, S_V, S_H) components on the basis of theoretical back-azimuth and incident angle (Farra and Vinnik, 2000). The L component is in the propagation direction of the incident S-wave, primarily containing S_p energy and nearly zero direct S-wave energy for horizontally layered homogeneous media. The Q component, which is perpendicular to the L component, contains significant direct S_V-wave energy that can partially convert to P-wave at sharp wave speed discontinuities (Farra and Vinnik, 2000). The rotated seismograms are time-reversed so that the S_p wave arrives after the direct S-wave and the crustal multiples prior to the S-wave. Subsequently, the L component is deconvolved in the time-domain by the S signal on the Q component to generate SRFs for the purpose of eliminating the influence of the source (Langston, 1979; Kumar et al., 2012). The arrival time of the S_p wave in the SRFs depends on the depth of the discontinuity, the wave speeds in the overlying layer, and the ray parameter of the direct S-wave, whereas its amplitude is proportional to the wave speed contrast across and the sharpness of the discontinuity.

The procedure to moveout correct and stack the SRFs follows the common conversion point (CCP) technique (Dueker and Sheehan, 1997), and is similar to the one that Gao and Liu (2014) used for imaging the mantle transition zone discontinuities across the contiguous U.S. To remove the influence of the ray parameter on the arrival times, moveout correction is applied prior to stacking the SRFs using (Sheriff and Geldart, 1982; Dueker and Sheehan, 1997)

$$T_{Sp} - T_S = \int_{-h}^{0} \left[\sqrt{(V_s(z)^{-2} - p^2} - \sqrt{V_p(z)^{-2} - p^2}\right] dz, \qquad (1)$$

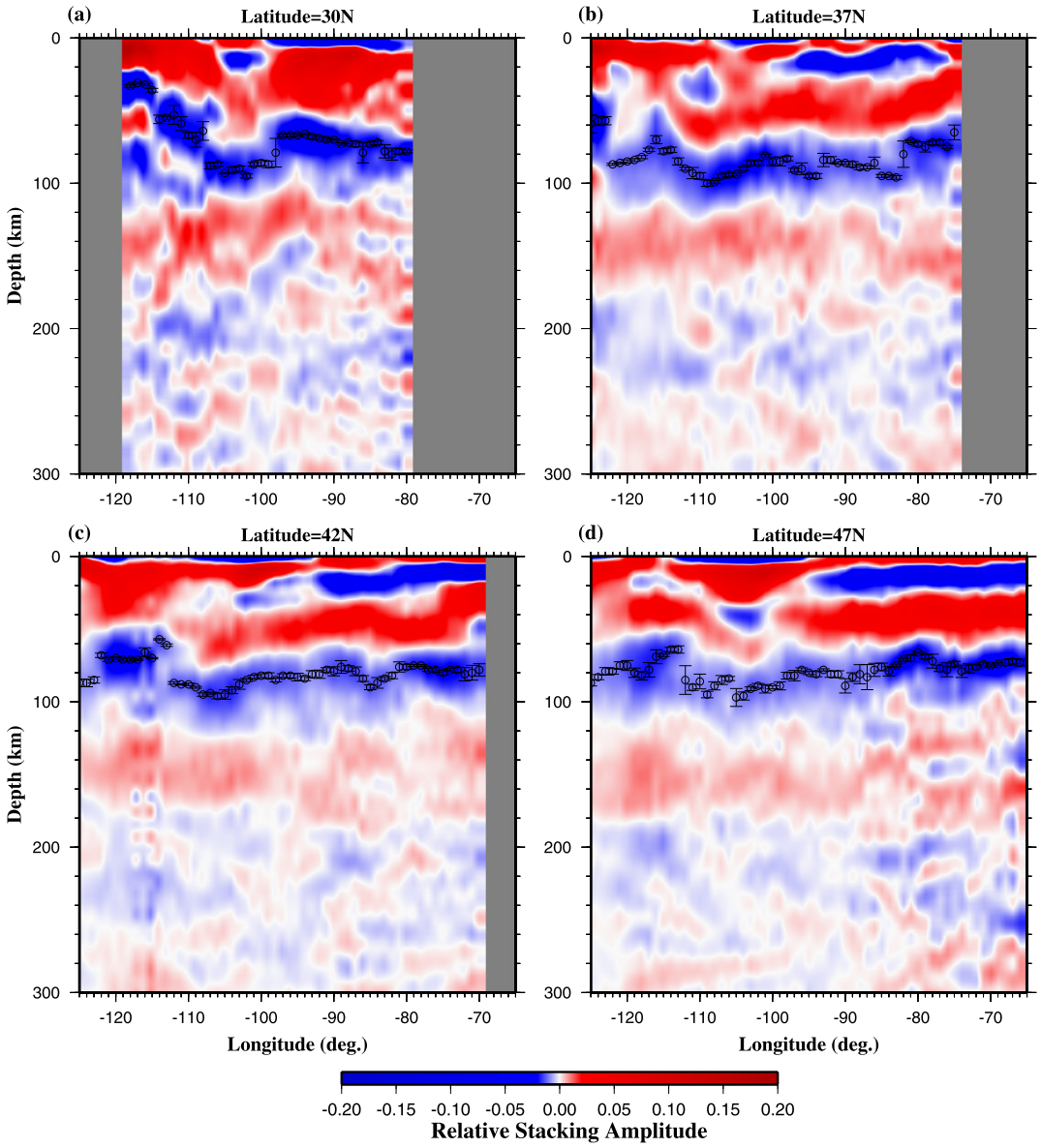

Fig. 2. Example plots of cross-sections along four latitudinal lines. The black circles mark the picked depth of the NVD. Similar plots for all the 27 latitudinal lines can be found in Fig. S1.

where p is the S-wave ray parameter, h is the depth of the candidate discontinuity which ranges from 0 to 300 km with an interval of 1 km, $V_p(z)$ and $V_s(z)$ are P and S-wave speeds, respectively, at depth z which are taken as the same as those in the IASP91 Earth model (Kennett and Engdahl, 1991). The SRFs are grouped into 2°-radius circular bins according to the location of the ray-piercing points computed based on the IASP91 Earth model. The distance between the center of neighboring bins is 1°. The SRFs in each of the bins are then moveout-corrected according to Eq. (1) and stacked to form a depth series with a vertical resolution of 1 km. To ensure reliability, bins with less than 50 SRFs are not used. The mean and standard deviation (SD) of the resulting NVD depth are obtained through bootstrap resampling with 10 iterations. While a higher number of iterations can lead to more accurately determined mean and SD, the large number of SRFs involved in the computation requires about a week-long computation time for each iteration under today's CPU clock rate and especially the input/output rate of the storage device. More importantly, the NVD arrival for the vast majority of the bins is unambiguously identified (Figs. 2 and S1), and therefore increasing the number of bootstrap iterations would unlikely lead to significantly different results.

3. Results

Totally 284,121 SRFs from 5,952 teleseismic events are used in the study. The number of SRFs per bin varies from 63 to 40,852 (Fig. 1). In comparison, the number of SRFs used by Hansen et al. (2015) for the central and western U.S. is 41,200, and that by Kumar et al. (2012) for the contiguous U.S. is 35,085. The edges of the study area are sampled by fewer SRFs, resulting in lower reliability than the interior. Fig. 2 shows examples of E-W cross-sections, and all the cross-sections with an interval of 1° can be found in Fig. S1, in which an NVD is observed corresponding to a robust negative arrival at the depth range of 30–110 km virtually in all the bins.

The depths of the NVD and the corresponding stacking amplitudes (Table S1) show systematic spatial variations, with mean values of 79 ± 13 km and 0.018 ± 0.009 over the study area, respectively (Fig. 3). In the following, these values are referred to

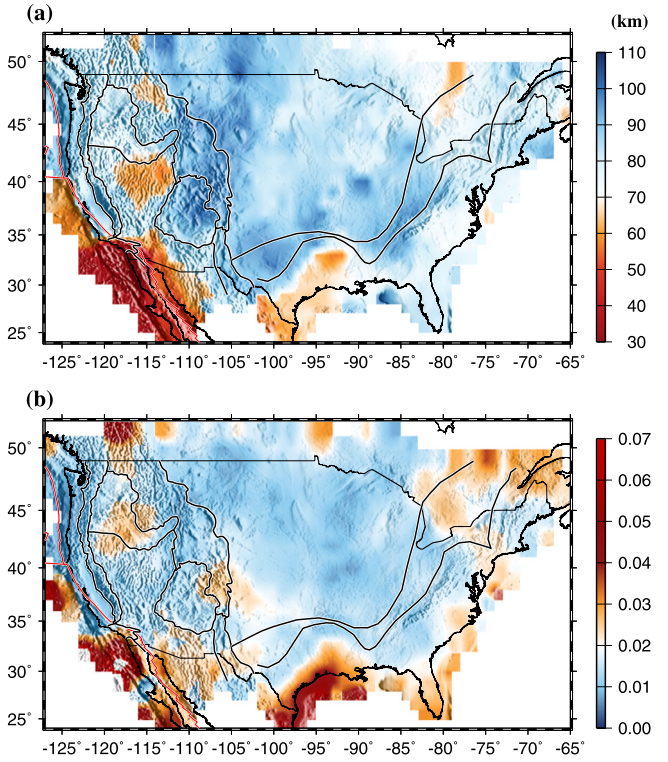

Fig. 3. (a) Resulting depth distribution of the negative wave speed discontinuity. (b) Distribution of stacking amplitudes (relative to that of the direct S-wave) for the NVD.

as normal values. The tectonically active western U.S. west of the Rocky Mountains, the Colorado Plateau, and the Rio Grande Rift is dominated by shallow (30–90 km) and spatially varying NVD depths, which are in agreement with most previous SRF studies (Kumar et al., 2012; Lekić and Fischer, 2014; Hansen et al., 2015). The Basin and Range Province and the area adjacent to the Gulf of California have the smallest depths (as low as ∼30 km) and relatively high amplitude (>0.02), which are consistent with the measurements of Reeves et al. (2015). The NVD beneath the Coast Ranges is the deepest and the corresponding amplitude is the smallest in the western U.S. (∼90 km and ∼0.01, respectively), both are comparable to those observed beneath the central U.S. NVD depths and amplitudes that are similar to the average over the study area are also found beneath the Columbia Plateau.

The Rocky Mountains and the neighboring Colorado Plateau are characterized by the deepest NVD in the whole study area, with a mean value of 95 ± 3 km. This is in agreement with the results of Levander and Miller (2012) who report a mean of ∼100 km. They are also consistent with the measurements of Kumar et al. (2012) and Hansen et al. (2015) for this study. The stacking amplitude in this area shows variable spatial distributions from 0.01 to 0.03.

The central U.S. demonstrates NVD depths ranging from 73 to 108 km, with an average of 87 ± 6 km. The depths of the NVD in the area have small spatial undulations, except for a few isolated areas such as the Llano Plateau in north-central Texas and the Southern Illinois Basin. The NVD depths are consistent with the measurements of Kumar et al. (2012), but are shallower than the results of Hansen et al. (2015), which show NVD depths of more than 160 km. Stacking amplitudes that are about half of those beneath the western U.S. are found in this area.

Anomalously shallow NVD depths and high stacking amplitudes are observed beneath the Texas–Louisiana Gulf Coastal Plain, in a coast-parallel band of about 200 km wide. The depths and amplitudes are spatially consistent within this band with a mean value of 63 ± 5 km and 0.030 ± 0.002, respectively. The NVD depth is significantly shallower than the ∼110 km found by previous studies (Kumar et al., 2012; Hansen et al., 2015).

Slightly shallower than normal depths are revealed beneath the Grenville and Appalachian provinces of the eastern U.S., as well as the northeastern corner of the central U.S. The depths range from 61 to 92 km, with an average of 76 ± 5 km. The NVD depths are consistent with SRF results obtained at isolated stations in the eastern U.S. (Rychert et al., 2007; Abt et al., 2010). The amplitudes in this region are in the range of 0.01–0.03 with an average of 0.023 ± 0.005, and are comparable to those in the western U.S.

The above depths were estimated based on the 1-D IASP91 Earth model and therefore the NVD depths are apparent rather than true depths. The uncertainty due to wave speed perturbation in the depths can be estimated using Equation (2) in Gao and Liu (2014). For areas with a shallow NVD in the western and eastern U.S., under the assumption that there is a mean V_s anomaly of −5% for the layer above the NVD (Schaeffer and Lebedev, 2014), an apparent depth of 60 km, and a V_s and V_p relative wave speed anomaly ratio of 2.0 (Gao and Liu, 2014), the estimated true depth is about 55 km. Similarly, for the central U.S., when the corresponding values of +4%, 90 km, and 1.8 are used, the estimated true depth is 96 km. The conclusion from the estimates is that in spite of the differences in the spatial distribution of the wave speeds in previous seismic tomography studies and in the V_s and V_p anomaly ratio, there is a possible bias in the estimated apparent depths of about 5 km. However, the contrast of the NVD depths between the central U.S. and the surrounding areas would be even more obvious in the corrected depths.

4. Discussion

4.1. Synthetic test

Due to the strong downward wave speed increase (about 24% for V_p and 19% for V_s) across the Moho (Kennett and Engdahl, 1991), there is a robust positive arrival in the resulting SRFs corresponding to the Moho. With limited band-width, a side-lobe may exist and could be misidentified as the NVD (e.g., Li et al., 2007; Kumar et al., 2012; Hansen et al., 2015). To investigate this possibility, we produce about 2,000 synthetic seismograms with randomly assigned focal parameters (focal depth, epicentral distance, and focal mechanisms) using the Complete Ordered Ray Expansion (CORE) suite of programs (Clarke, 1993). The input 1-D model includes a 35 km thick crust, the 410 and 660 km discontinuities, and the core–mantle boundary. The wave speeds and densities are the same as those in the IASP91 Earth model. The synthetic seismograms are then processed and stacked using exactly the same procedures as those used for the real data.

The resulting depth series produced using the synthetic SRFs (Fig. 4a) indeed possesses a negative arrival beneath the positive one corresponding to the Moho. However, comparing with the depth series created using the observed data (Fig. 4b), several differences can be observed. First, on the synthetic result, the ratio between the depth of the negative arrival beneath the Moho and the depth of the Moho (Fig. S2) is about 1.8, while it varies systematically from 1.0 to 4.6 across the study area (Fig. 5a). Even when possible lateral variations in crustal wave speeds are considered, it is unlikely that the depth of the Moho side-lobe can display such variability. Second, the ratio between the amplitudes of the sub-Moho negative arrival and the Moho arrival (Fig. S2) is about 0.4 on the synthetic trace, while that for the observed data is mostly greater than 0.4 and can be as large as 4.0 (Fig. 5b). Third, while the two side-lobes on the synthetic trace are symmetric with regard to the peak of the Moho arrival, the two negative arrivals on most of the observed traces are asymmetric, with the lower one being significantly more separated from the Moho arrival (Fig. 4).

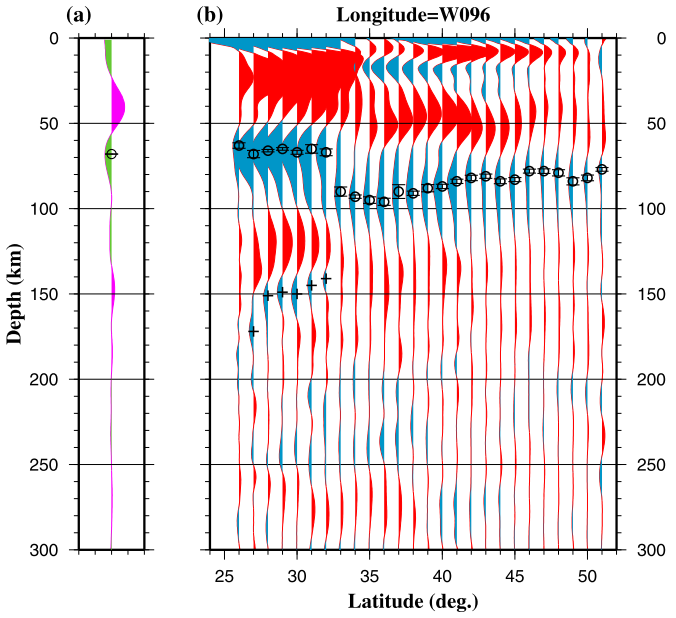

Fig. 4. (a) Depth series from CORE synthetic seismograms. (b) Observed depth series along an N-S profile following the 96°W longitudinal line. The circles in the depth range of 60–100 km mark the NVD, and the pluses at the southern part of the profile indicate a negative arrival possibly representing the LAB beneath the Texas Coastal Plain. The amplitudes for traces in (a) and (b) are on the same scale.

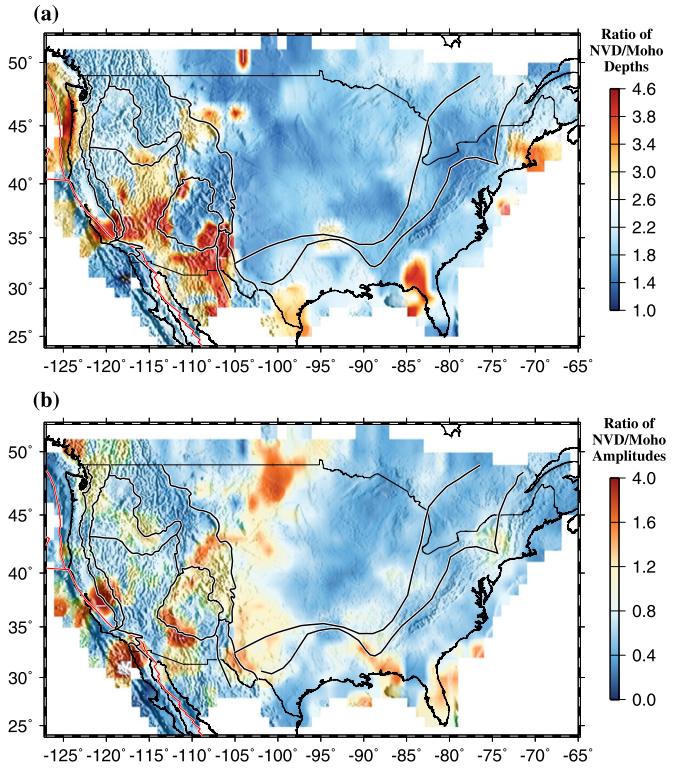

Fig. 5. (a) Ratio of the depths of the observed NVD and the Moho. (b) Ratio of stacking amplitudes corresponding to the NVD and the Moho.

Therefore, the result of the synthetic test is inconsistent with the possibility that the NVD is a side-lobe of the Moho arrival on the SRFs. Instead, it represents a real negative discontinuity in the upper mantle.

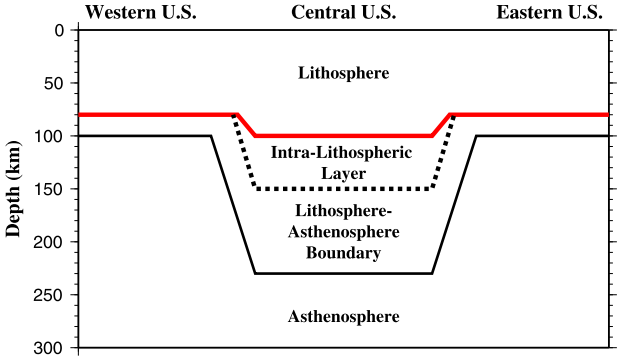

Fig. 6. A schematic model illustrating the stratification of the lithosphere along an E-W profile across the study area. The red line is the SRF-detected boundary.

4.2. A shallow and sharp LAB in the western U.S.

The mean depth (69 ± 17 km) of the NVD observed beneath the western U.S. is comparable to the depth of the bottom of the rigid lithosphere revealed from seismic surface wave tomography (McKenzie and Priestley, 2008; Schaeffer and Lebedev, 2014) and the depth of the LAB inferred from mantle xenolith data (Mareschal and Jaupart, 2004). Therefore, similar to previous SRF studies (e.g., Kumar et al., 2012; Lekić and Fischer, 2014; Hansen et al., 2015), we consider this discontinuity to be the sharp LAB (Figs. 6 and S3). This interpretation of the NVD is consistent with the inferred anomalously high temperature of 1200 °C at the depth of about 80 km beneath the western U.S. (Hansen et al., 2015).

In the area adjacent to the Gulf of California, the depth of the LAB is the shallowest (30–50 km) in the entire study area, and the crustal thickness varies from 20 to 25 km (Yan and Clayton, 2007; Zhu and Kanamori, 2000). The thinning of both the crust and sub-crustal lithosphere beneath the Gulf of California and adjacent areas is consistent with the hypothesis of strain-localization-induced lithospheric thinning, probably originating from the clockwise rotation of the Transverse Range (Lekić et al., 2011; Reeves et al., 2015).

Another area with thin lithosphere (~60 km) in the western U.S. is the Basin and Range Province (BRP), which is characterized by crustal thinning as well. For the BRP, there are two possible mechanisms contributing to the thinning of the lithosphere, including removal of the lower part of the lithosphere by the Farallon flat-lying subduction (Cox et al., 2016), and middle to late Cenozoic continental extension (Zandt et al., 1995; Lekić and Fischer, 2014). With an average crustal thickness of 25 km and 50 km beneath the BRP and the Colorado Plateau, respectively, the crustal stretch rate of the BRP is 60–100% based on previous studies (Zandt et al., 1995; Bashir et al., 2011). Comparing with our observations of lithospheric thickness beneath the BRP (50–70 km) and the neighboring Colorado Plateau (90–110 km), the amount of thinning of the sub-crustal lithosphere is approximately proportional to that of the crust if we assume that the pre-stretching lithospheric thickness was comparable beneath the Plateau and surrounding areas. Therefore, uniform lateral stretching of the entire lithosphere seems to be a viable cause of the observed lithospheric thinning.

The thickest lithosphere and smallest stacking amplitudes in the western U.S. are observed beneath the Cascade Range-Sierra Nevada, which is mostly located above the subducted Juan De Fuca slab. The reduced wave speed contrast across the LAB beneath this area, as reflected by the small stacking amplitudes, might be caused by partial melting within the lithospheric mantle induced by the hydrous oceanic slab (Walowski et al., 2016). Dehydration reactions have been recognized by previous studies (Walowski et al., 2016), and flux melting of the crust of the Juan De Fuca slab

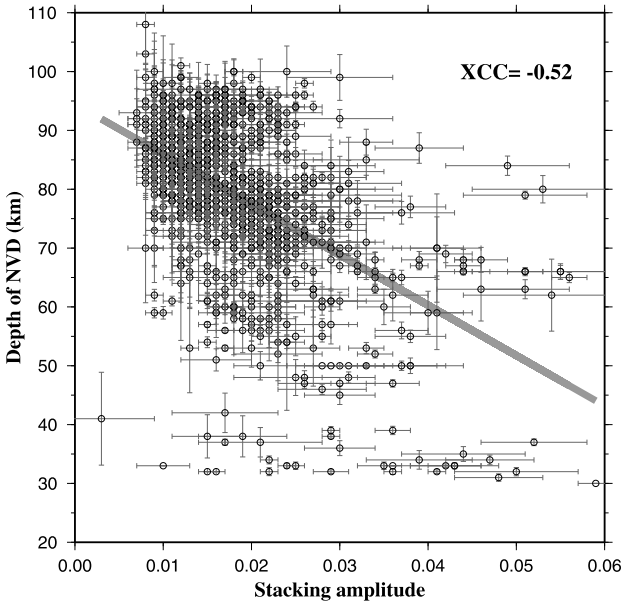

Fig. 7. Depths of the NVD plotted against the corresponding stacking amplitudes for stations in the Western U.S. XCC: cross correlation coefficient.

may have migrated into the overlying mantle of the North American plate, resulting in melting in the lower lithosphere, which in turn may reduce mantle wave speeds and result in the observed small stacking amplitudes.

In general, beneath the western U.S., areas with thin lithosphere possess large stacking amplitudes and vice versa (Fig. 7). One of the simplest explanations for this relationship is a higher degree of partial melting in the top-most layer of the asthenosphere beneath thinner lithosphere, leading to a greater wave speed contrast between the lithosphere and asthenosphere. Under the assumption that the bottom of the lithosphere is a constant temperature interface, the lower pressure corresponding to a thinner lithosphere leads to a higher degree of partial melting (e.g., Ganguly, 2005). Experimental and modeling studies suggest that melting can be induced by the presence of volatiles (Green et al., 2010) and by a dramatic reduction in water solubility of aluminous orthopyroxene (Mierdel et al., 2007).

4.3. An intra-lithospheric low wave speed layer beneath the central U.S.

Most seismic surface wave tomography studies suggest that beneath the cratonic region of the central U.S., the thickness of the lithosphere is about 250 km and can be further divided into various sub-layers (McKenzie and Priestley, 2008; Bedle and van der Lee, 2009; Yuan and Romanowicz, 2010; Schaeffer and Lebedev, 2014). Therefore, the NVD observed at the average depth of 87 ± 6 km beneath this area is a mid-lithospheric discontinuity. Combining previous results of mantle temperature (Hansen et al., 2015) and shear wave speed (Abt et al., 2010; Yuan and Romanowicz, 2010) with the weaker amplitude corresponding to the NVD relative to that of the western U.S. obtained in this study (Fig. 3b), this discontinuity may represent the top boundary of a 40–60 km thick low wave speed intra-lithospheric layer (ILL; Figs. 6 and S3). This interpretation is consistent with the lithospheric layering model obtained from joint inversion of long and short period seismic data (Caló et al., 2016), which detected double MLDs at depths of about 100–130 and 150–170 km, indicating the top and bottom of a low wave speed ILL. The 70-km-wide thermal root is a gradual instead of sharp LAB between the bottom of the ILL and the underlain asthenosphere (Fig. 6).

Several formation mechanisms have been proposed for this sharp MLD, including 1) high geothermal gradients or presence of partial melt (Yuan and Romanowicz, 2010; Kumar et al., 2012); 2) variation in the geometry of seismic anisotropy, from diffusion/superplastic to dislocation creep (Rychert and Shearer, 2009; Ford et al., 2016); and 3) compositional variation caused by metasomatism or crystallized melts, e.g., volatile, chemical depletion or low wave speed minerals such as amphibole and phlogopite (Griffin et al., 2004; Foster et al., 2014; Hansen et al., 2015; Hopper and Fischer, 2015). In-depth discussions of the above mechanisms can be found in Hansen et al. (2015), who concluded that the ILL is most likely a compositionally distinct layer that is rich in phlogopite.

4.4. Lithospheric extension in the Texas–Louisiana Gulf Coastal Plain

The Gulf Coastal Plain has undergone several complicated geological processes, such as collision, extension, and rifting (Evanzia et al., 2014). The shallow but strong NVD observed at the depth of ~60 km beneath this area can be interpreted as a low wave speed layer within the lithosphere (Ainsworth et al., 2014), similar to the central U.S. If we assume that the original depth of this interface is the same as that beneath the central U.S. (~100 km), a stretching (β) factor of about 1.7 is obtained. This is comparable to the average crustal stretching factor (e.g., Mickus et al., 2009) and suggests that the shallowing of the NVD is the consequence of lithospheric extension. An alternative explanation of the shallow NVD is that it is the result of an upward propagation of a metasomatic front associated with increased heat-flow in areas with continental extension (Thibault et al., 1992; Hansen et al., 2015).

Beneath this area, another negative signal is observed at the depth of ~150 km (Fig. 4b). It is not seen on the synthetic trace (Fig. 4a) and thus is unlikely to be an artifact (which is possibly the case for the positive arrival above the negative one which appears on the synthetic trace at the depth of about 150 km). This discontinuity has also been observed by previous studies (Kumar et al., 2012; Ainsworth et al., 2014; Hansen et al., 2015) and could be interpreted as representing the bottom of the rigid lithosphere. Under the assumption that the pre-stretching lithospheric thickness is similar to that beneath the central U.S. (~250 km), the β factor for the lithosphere is ~1.7, which is the same as the β factor computed using the depth of the NVD. Note that relative to the western half of the Coastal Plain, the eastern part (east of 90°W) shows much smaller stretching.

4.5. Lithospheric modification in the eastern U.S.

The depth and amplitude of the NVD beneath the eastern U.S. are similar to those observed beneath the tectonically active western U.S. Based on the similarities between the SRF-revealed and tomographically-determined depths, we consider the NVD to represent a sharp LAB, as proposed by previous SRF studies (Rychert et al., 2007; Abt et al., 2010). Beneath the northeastern U.S., the LAB is notably shallower (~70 km) and the amplitude is higher (~0.03) than those of the neighboring regions (Fig. 3). In this area, a low wave speed anomaly at the base of the lithosphere, referred to as an indentation or Great Lakes mantle divot, has been suggested by seismic tomographic studies, and was regarded as the consequence of mantle plume accumulation (Bedle and van der Lee, 2009; Burdick et al., 2017). The observed thinning of the lithosphere (Fig. 3a) could be the result of lithosphere–plume interaction (Eaton and Frederiksen, 2007), and the increased wave speed contrast between the bottom of the eroded lithosphere and the underlying mantle plume material can explain the observed high stacking amplitudes beneath this area (Fig. 3b).

5. Conclusions

A robust negative wave speed discontinuity is pervasively detected in the contiguous U.S. in the depth range of 30–110 km in consecutive 2° circular bins using a high number of S receiver functions that is unprecedented for the study area. Beneath the extended crust of the western U.S., the Gulf Coastal Plain, and the eastern U.S., similarities between the depth of the this discontinuity and depths of the LAB revealed by seismic tomography and xenolith studies suggest that it represents the sharp boundary between the cold lithosphere and the partially melted asthenosphere. In contrast, beneath the stable cratonic region of the central U.S., this discontinuity is most likely the sharp upper boundary of a chemically distinct layer probably formed by metasomatism in the ancient lithosphere. Further investigations are needed in order to understand the contrasting thickness of the LAB between the cratonic central U.S. and the adjacent younger areas.

An intriguing anti-correlation between the depth of the negative wave speed discontinuity and the amplitude of the S_p wave is revealed for the western U.S. One of the simplest explanations for this relationship is that the top-most layer of the asthenosphere experiences more volatile-induced melting beneath thinner lithosphere. Uniform extension of the lithosphere in the Basin and Range Province and the Texas–Louisiana Gulf Coastal Plain can satisfactorily explain the observed thinning of the crust and the whole lithosphere. Finally, anomalously thin lithosphere and large stacking amplitudes observed beneath the northeastern U.S. may indicate erosion of the bottom of the lithosphere, probably by a passing mantle plume.

Acknowledgements

All the data used in the study were obtained from the IRIS DMC (last accessed: Jan 2016) which is funded through the Seismological Facilities for the Advancement of Geoscience and EarthScope (SAGE) Proposal of the National Science Foundation under Cooperative Agreement EAR-1261681. This study was partially supported by the China Scholarship Council to L.L. under contract 201408040006, and the United States National Science Foundation under grant 1460516 to S.G.

Appendix A. Supplementary material

Supplementary material related to this article can be found online at https://doi.org/10.1016/j.epsl.2018.05.012.

References

Abt, D.L., Fischer, K.M., French, S.W., Ford, H.A., Yuan, H., Romanowicz, B., 2010. North American lithospheric discontinuity structure imaged by P_s and S_p receiver functions. J. Geophys. Res. 115 (B9). https://doi.org/10.1029/2009JB006914.

Ainsworth, R., Pulliam, J., Gurrola, H., Evanzia, D., 2014. S_p receiver function imaging of a passive margin: transect across Texas's Gulf Coastal Plain. Earth Planet. Sci. Lett. 402, 138–147. https://doi.org/10.1016/j.epsl.2014.05.056.

Bashir, L., Gao, S.S., Liu, K.H., Mickus, K., 2011. Crustal structure and evolution beneath the Colorado Plateau and the southern Basin and Range Province: results from receiver function and gravity studies. Geochem. Geophys. Geosyst. 12 (6). https://doi.org/10.1029/2011GC003563.

Bedle, H., van der Lee, S., 2009. S velocity variations beneath North America. J. Geophys. Res. 114 (B7). https://doi.org/10.1029/2008JB005949.

Burdick, S., Vernon, F.L., Martynov, V., Eakins, J., Cox, T., Tytell, J., Mulder, T., White, M.C., Astiz, L., Pavlis, G.L., van der Hilst, R.D., 2017. Model update May 2016: upper-mantle heterogeneity beneath North America from travel-time tomography with global and USArray data. Seismol. Res. Lett. 88 (2A), 319–325. https://doi.org/10.1785/0220160186.

Caló, M., Bodin, T., Romanowicz, B., 2016. Layered structure in the upper mantle across North America from joint inversion of long and short period seismic data. Earth Planet. Sci. Lett. 499, 164–175. https://doi.org/10.1016/j.epsl.2016.05.054.

Clarke, T.J., 1993. The complete ordered ray expansion-II. Multiphase body wave tomography. Geophys. J. Int. 115 (2), 435–444. https://doi.org/10.1111/j.1365-246X.1993.tb01197.x.

Cox, P., Stubailo, I., Davis, P., 2016. Receiver function and geometric tomography along the Monterey microplate to test slab delamination or lithospheric drip models of the Isabella Anomaly, California. Bull. Seismol. Soc. Am. 106 (1), 267–280. https://doi.org/10.1785/0120140339.

Dueker, K.G., Sheehan, A.F., 1997. Mantle discontinuity structure from midpoint stacks of converted P to S waves across the Yellowstone hotspot track. J. Geophys. Res. 102, 8313–8327.

Eaton, D.W., Frederiksen, A., 2007. Seismic evidence for convection-driven motion of the North American plate. Nature 446 (7134), 428–431. https://doi.org/10.1038/nature05675.

Evanzia, D., Pulliam, J., Ainsworth, R., Gurrola, H., Pratt, K., 2014. Seismic Vp & Vs tomography of Texas & Oklahoma with a focus on the Gulf Coast margin. Earth Planet. Sci. Lett. 402, 148–156. https://doi.org/10.1016/j.epsl.2013.12.027.

Faber, S., Müller, G., 1980. S_p phases from the transition zone between the upper and lower mantle. Bull. Seismol. Soc. Am. 70 (2), 487–508.

Farra, V., Vinnik, L., 2000. Upper mantle stratification by P and S receiver functions. Geophys. J. Int. 141 (3), 699–712. https://doi.org/10.1046/j.1365-246x.2000.00118.x.

Fischer, K.M., Ford, H.A., Abt, D.L., Rychert, C.A., 2010. The lithosphere–asthenosphere boundary. Annu. Rev. Earth Planet. Sci. 38, 551–575. https://doi.org/10.1146/annurev-earth-040809-152438.

Ford, H.A., Long, M.D., Wirth, E.A., 2016. Midlithospheric discontinuities and complex anisotropic layering in the mantle lithosphere beneath the Wyoming and Superior Provinces. J. Geophys. Res. 121 (9), 6675–6697. https://dx.doi.org/10.1002/2016JB012978.

Foster, K., Dueker, K., Schmandt, B., Yuan, H., 2014. A sharp cratonic lithosphere–asthenosphere boundary beneath the American Midwest and its relation to mantle flow. Earth Planet. Sci. Lett. 402, 82–89. https://doi.org/10.1016/j.epsl.2013.11.018.

Ganguly, J., 2005. Adiabatic decompression and melting of mantle rocks: an irreversible thermodynamic analysis. Geophys. Res. Lett. 32 (6). https://doi.org/10.1029/2005GL022363.

Gao, S.S., Liu, K.H., 2014. Mantle transition zone discontinuities beneath the contiguous United States. J. Geophys. Res. 119, 6452–6468. https://doi.org/10.1002/2014JB011253.

Green, D.H., Hibberson, W.O., Kovács, I., Rosenthal, A., 2010. Water and its influence on the lithosphere–asthenosphere boundary. Nature 467, 448–451. https://doi.org/10.1038/nature09369.

Griffin, W.L., O'Reilly, S.Y., Doyle, B.J., Pearson, N.J., Coopersmith, H., Kivi, K., Malkovets, V., Pokhilenko, N., 2004. Lithosphere mapping beneath the North American plate. Lithos 77 (1), 873–922. https://doi.org/10.1016/j.lithos.2004.03.034.

Hansen, S.M., Dueker, K., Schmandt, B., 2015. Thermal classification of lithospheric discontinuities beneath USArray. Earth Planet. Sci. Lett. 431, 36–47. https://doi.org/10.1016/j.epsl.2015.09.009.

Hoffman, P.F., 1988. United plates of America, the birth of a craton: early Proterozoic assembly and growth of Laurentia. Annu. Rev. Earth Planet. Sci. 16 (1), 543–603. https://doi.org/10.1146/annurev.ea.16.050188.002551.

Hopper, E., Fischer, K.M., 2015. The meaning of midlithospheric discontinuities: a case study in the northern US craton. Geochem. Geophys. Geosyst. 16 (12), 4057–4083. https://doi.org/10.1002/2015GC006030.

Kennett, B.L.N., Engdahl, E.R., 1991. Traveltimes for global earthquake location and phase identification. Geophys. J. Int. 105 (2), 429–465. https://doi.org/10.1111/j.1365-246X.1991.tb06724.x.

Kind, R., Yuan, X., Kumar, P., 2012. Seismic receiver functions and the lithosphere–asthenosphere boundary. Tectonophysics 536, 25–43. https://doi.org/10.1016/j.tecto.2012.03.005.

Kumar, P., Kind, R., Yuan, X., Mechie, J., 2012. USArray receiver function images of the lithosphere–asthenosphere boundary. Seismol. Res. Lett. 83 (3), 486–491. https://doi.org/10.1785/gssrl.83.3.486.

Langston, C.A., 1979. Structure under Mount Rainier, Washington, inferred from teleseismic body waves. J. Geophys. Res. 84 (B9), 4749–4762. https://dx.doi.org/10.1029/JB084iB09p04749.

Lekić, V., Fischer, K.M., 2014. Contrasting lithospheric signatures across the western United States revealed by S_p receiver functions. Earth Planet. Sci. Lett. 402, 90–98. https://doi.org/10.1016/j.epsl.2013.11.026.

Lekić, V., French, S.W., Fischer, K.M., 2011. Lithospheric thinning beneath rifted regions of Southern California. Science 334 (6057), 783–787. https://doi.org/10.1126/science.1208898.

Levander, A., Miller, M.S., 2012. Evolutionary aspects of lithosphere discontinuity structure in the western US. Geochem. Geophys. Geosyst. 13 (7). https://doi.org/10.1029/2012GC004056.

Li, X., Yuan, X., Kind, R., 2007. The lithosphere–asthenosphere boundary beneath the western United States. Geophys. J. Int. 170 (2), 700–710. https://doi.org/10.1111/j.1365-246X.2007.03428.x.

Liu, K.H., Gao, S.S., 2010. Spatial variations of crustal characteristics beneath the Hoggar swell, Algeria, revealed by systematic analyses of receiver functions from

a single seismic station. Geochem. Geophys. Geosyst. 11 (8). http://doi.org/10.1029/2010GC003091.

Liu, L., Gao, S.S., Liu, K.H., Mickus, K., 2017. Receiver function and gravity constraints on crustal structure and vertical movements of the Upper Mississippi Embayment and Ozark Uplift. J. Geophys. Res. 122, 4572–4583. https://doi.org/10.1002/2017JB014201.

Mareschal, J.C., Jaupart, C., 2004. Variations of surface heat flow and lithospheric thermal structure beneath the North American craton. Earth Planet. Sci. Lett. 223 (1), 65–77. https://doi.org/10.1016/j.epsl.2004.04.002.

McKenzie, D., Priestley, K., 2008. The influence of lithospheric thickness variations on continental evolution. Lithos 102 (1), 1–11. https://doi.org/10.1016/j.lithos.2007.05.005.

Mickus, K., Stern, R.J., Keller, G.R., Anthony, E.Y., 2009. Potential field evidence for a volcanic rifted margin along the Texas Gulf Coast. Geology 37 (5), 387–390. https://doi.org/10.1130/G25465A.1.

Mierdel, K., Keppler, H., Smyth, J.R., Langenhorst, F., 2007. Water solubility in aluminous orthopyroxene and the origin of Earth's asthenosphere. Science 315 (5810), 364–368. https://doi.org/10.1126/science.1135422.

Murphy, B.S., Egbert, G.D., 2017. Electrical conductivity structure of southeastern North America: implications for lithospheric architecture and Appalachian topographic rejuvenation. Earth Planet. Sci. Lett. 462, 66–75. https://doi.org/10.1016/j.epsl.2017.01.009.

Reeves, Z., Lekić, V., Schmerr, N., Kohler, M., Weeraratne, D., 2015. Lithospheric structure across the California Continental Borderland from receiver functions. Geochem. Geophys. Geosyst. 16 (1), 246–266. https://doi.org/10.1002/2014GC005617.

Rychert, C.A., Shearer, P.M., 2009. A global view of the lithosphere–asthenosphere boundary. Science 324 (5926), 495–498. https://doi.org/10.1126/science.1169754.

Rychert, C.A., Rondenay, S., Fischer, K.M., 2007. P-to-S and S-to-P imaging of a sharp lithosphere–asthenosphere boundary beneath eastern North America. J. Geophys. Res. 112 (B8). https://doi.org/10.1029/2006JB004619.

Schaeffer, A.J., Lebedev, S., 2014. Imaging the North American continent using waveform inversion of global and USArray data. Earth Planet. Sci. Lett. 402, 26–41. https://doi.org/10.1016/j.epsl.2014.05.014.

Sheriff, R.E., Geldart, L.P., 1982. Exploration Seismology. Vol. 1: History, Theory, and Data Acquisition. Cambridge University Press, Cambridge.

Thibault, Y., Edgar, A.D., Lloyd, F.E., 1992. Experimental investigation of melts from a carbonated phlogopite lherzolite: implications for metasomatism in the continental lithospheric mantle. Am. Mineral. 77, 784–794.

Walowski, K.J., Wallace, P.J., Clynne, M.A., Rasmussen, D.J., Weis, D., 2016. Slab melting and magma formation beneath the southern Cascade arc. Earth Planet. Sci. Lett. 446, 100–112. https://doi.org/10.1016/j.epsl.2016.03.044.

Yan, Z., Clayton, R.W., 2007. Regional mapping of the crustal structure in southern California from receiver functions. J. Geophys. Res. 112 (B5). https://doi.org/10.1029/2006JB004622.

Yang, B.B., Gao, S.S., Liu, K.H., Elsheikh, A.A., Lemnifi, A.A., Refayee, H.A., Yu, Y., 2014. Seismic anisotropy and mantle flow beneath the northern Great Plains of North America. J. Geophys. Res. 119 (3), 1971–1985. https://doi.org/10.1002/2013JB010561.

Yuan, H., Romanowicz, B., 2010. Lithospheric layering in the North American craton. Nature 466 (7310), 1063–1068. https://doi.org/10.1038/nature09332.

Zandt, G., Myers, S.C., Wallace, T.C., 1995. Crust and mantle structure across the Basin and Range-Colorado Plateau boundary at 37°N latitude and implications for Cenozoic extensional mechanism. J. Geophys. Res. 100, 10529–10548. https://doi.org/10.1029/94JB03063.

Zhu, L., Kanamori, H., 2000. Moho depth variation in southern California from teleseismic receiver functions. J. Geophys. Res. 105 (B2), 2969–2980. https://doi.org/10.1029/1999JB900322.